Second-moment interatomic potential for Cu-Au alloys based on total-energy calculations and its application to molecular-dynamics simulations

1998 J. Phys.: Condens. Matter 10 10979

(http://iopscience.iop.org/0953-8984/10/48/018)

J. Phys.: Condens. Matter **10** (1998) 10979–10990. Printed in the UK PII: S0953-8984(98)96177-X

Second-moment interatomic potential for Cu–Au alloys based on total-energy calculations and its application to molecular-dynamics simulations

N I Papanicolaou†§, G C Kallinteris†, G A Evangelakis†, D A Papaconstantopoulos†‡ and M J Mehl‡

† Department of Physics, Solid State Division, University of Ioannina, PO Box 1186, GR-45110 Ioannina, Greece

‡ Complex Systems Theory Branch, Naval Research Laboratory, Washington, DC 20375-5345, USA

Received 23 July 1998

Abstract. We have evaluated interatomic potentials of Cu, Au and Cu–Au $L1_2$ ordered alloys in the framework of the second-moment approximation to the tight-binding theory by fitting to the volume dependence of the total energy of these materials computed by first-principles augmented-plane-wave calculations. We have applied this scheme to calculate the bulk modulus and elastic constants of the pure elements and alloys and we have obtained a good agreement with experiment. We also have performed molecular-dynamics simulations at various temperatures, deducing the temperature dependence of the lattice constants and the atomic mean square displacements, as well as the phonon density of states and the phonon-dispersion curves of the ordered alloys. A satisfactory accuracy was obtained, comparable to previous works based on the same approximation, but resulting from fitting to various experimental quantities.

1. Introduction

Atomistic computer modelling has been developed over the last twenty years in condensed-matter and materials research, in order to offer a direct and unique microscopic view of a system [1–5]. The description of the atomic interactions (the so-called 'interatomic potential') plays a central role in any atomistic simulation, ranging from accurate first-principles electronic-structure techniques [6] to simple empirical schemes [7, 8]. It is recognized that fully self-consistent *ab initio* electronic structure methods are superior and highly accurate, but that they cannot be as efficient as empirical potentials for simulations requiring large systems and long time scales. The many-body potential schemes for metals and intermetallic alloys include the embedded-atom method [9], the effective medium theory [10], the Finnis–Sinclair potentials [11], the glue model [12] and the second-moment approximation (SMA) to the tight-binding (TB) model [13–15]. The above potentials, while simple, in many cases provide a good and quick description of the bonding and energetics in metallic systems. For this reason these potentials are still useful and should play a supplementary role to other more accurate techniques.

In the SMA scheme [14], the total cohesive energy of the system consists of a band term, proportional to the square root of the second moment of the density of states [16], and

§ Corresponding author: N I Papanicolaou. E-mail address: nikpap@cc.uoi.gr.

0953-8984/98/4810979+12$19.50

a repulsive pair-potential term which contains the non-band-structure parts of the energy, such as electrostatic and exchange–correlation interactions. The SMA expression of the total energy is based on a small set of empirical parameters that are usually determined by matching with experimental data, including the cohesive energy, lattice constant, bulk modulus and independent elastic constants of the system [15, 17]. The extension of the range of the potential includes a great number of interacting neighbours (typically up to fifth neighbours) and has been found to provide better and more realistic results compared to experiment [17–21].

Recently, the above approach has been applied to some binary cubic alloys of technological interest, such as Ni_3Al [17] and Cu_3Au [17, 22–26], aiming to describe their basic thermodynamical and structural properties. In these studies the parameters for the interactions between like atoms in the alloy have been assumed to be the same as in the respective pure metals. As a result, only the cross-interaction parameters have been fitted to the experimental data of the alloy. On the other hand, in previous studies [27] we presented an alternative and equally successful approach to parametrizing the expression for the total energy of noble metals within the SMA. In this case we did not use the experimental quantities of the metals (cohesive energy, lattice parameter and elastic constants); instead we fitted to the total energy obtained from first-principles augmented-plane-wave (APW) calculations as a function of volume.

The purpose of the present work is to extend the above alternative approach to binary alloys by developing an interatomic potential for Cu–Au alloys in the framework of the SMA model. The choice of that compound is based on the fact that it has often served as a prototypical system, showing order–disorder phase transition, bimetallic interface and two-dimensional alloys and therefore has been extensively investigated both experimentally and theoretically [28]. In order to validate the quality of our parameters, we calculated the bulk modulus and the elastic constants of pure metals and ordered alloys. Furthermore, we performed molecular-dynamics (MD) simulations at various temperatures and we obtained the variation of the lattice constants and the atomic mean square displacements (MSD) of the alloys as a function of the temperature. Finally, we derived the phonon density of states (DOS) and the phonon-dispersion curves of the alloys, which we compared with available experimental values.

The paper is organized as follows: in section 2 we describe the computational method, while the results and their comparison with experiment are discussed in section 3. The last section is devoted to conclusions.

2. Computational methodology

The electronic band structure of the noble metals Cu, Au (fcc structure) and their ordered alloys Cu_3Au, Au_3Cu ($L1_2$ structure) was calculated self-consistently by the APW method within the muffin-tin approximation [29]. We used the Hedin–Lundqvist parametrization [30] of the local-density approximation (LDA) [31] to density-functional theory [32]. The core levels were treated by a fully relativistic calculation as atomic levels in each iteration, while the outer 11 electrons of each element were treated as band electrons in the semirelativistic approximation [33] (neglecting spin–orbit coupling) on a mesh of 89 $\boldsymbol{k}$ and 35 $\boldsymbol{k}$ points in the irreducible Brillouin zone for the fcc and $L1_2$ structure respectively. The total energy was computed from Janak's expression [34] by using the resulting self-consistent crystal potential, charge density and the eigenvalue sum. We calculated the total energy for five different lattice constants and by a parabolic fitting [35] we determined the equilibrium lattice constant and the total-energy curve.

As has been noted in section 1, the total energy of the system, within the SMA model [14, 17], is written as:

$$E = -\sum_{i=1}^{N}\left(\sum_{j\neq i} A_{\alpha\beta}\exp\left[-p_{\alpha\beta}\left(\frac{r_{ij}}{r_0^{\alpha\beta}}-1\right)\right]-\left\{\sum_{j\neq i}\xi_{\alpha\beta}^2\exp\left[-2q_{\alpha\beta}\left(\frac{r_{ij}}{r_0^{\alpha\beta}}-1\right)\right]\right\}^{1/2}\right) \tag{1}$$

where the first sum corresponds to the pair-potential repulsive term of Born–Mayer type and the second sum to the band-structure term, which has a many-body character due to its square root form. In the expression (1), N is the number of the particles, r_{ij} is the distance between atoms i and j of the species α and β respectively (α, β stand for Cu or Au) and the sums over j are extended up to fifth neighbours. Usually $r_0^{\alpha\beta}$ is taken equal to the first-neighbour distance in the pure systems ($\alpha \equiv \beta$) and the alloys ($a \neq \beta$) [17, 22–26]. In the present case $r_0^{\alpha\beta}$ is taken to be three additional free parameters, which with the other 12 adjustable parameters $A_{\alpha\beta}$, $\xi_{\alpha\beta}$, $p_{\alpha\beta}$ and $q_{\alpha\beta}$ describe the interactions in the pure elements and in the stoichiometric alloys. These 15 parameters have been determined from the expression (1) by simultaneous fitting to the APW total-energy curves as a function of volume for the pure metals Cu, Au and the $L1_2$ alloys Cu_3Au, Au_3Cu. An attempt to also include the CuAu alloy in the fitting procedure did not give very good agreement with experiment for all the elastic constants and therefore we decided to deal with only the fcc-based alloys. The fits have been performed using the MERLIN package, which provides several minimization algorithms [36]. It should be noted that before the fitting procedure, we subtracted from each APW total-energy curve the corresponding energies of isolated atoms, calculated in the LDA by a relativistic formalism, i.e. we constructed the cohesive energy curves. Furthermore, we shifted the computed cohesive energy graphs uniformly, so that at the minimum each curve gives the experimental cohesive energy of the corresponding system, given that the total energy of isolated atoms is not sufficiently accurate within the LDA approach.

Using the expression (1) with the adjusted parameters, we calculated the bulk modulus of the metals and alloys by the method proposed in [35]. In addition, the elastic constants were calculated at the experimental lattice constant at room temperature by evaluating the total energy using an orthorhombic and a monoclinic strain on the lattices [37] and then determining the difference in total energies of the distorted and undistorted lattices.

Furthermore, we performed MD simulations for the ordered alloys in the canonical ensemble aiming to test the behaviour of this model and the quality of our parameters at finite temperatures. The system was made up of 4000 particles arranged on an fcc lattice. In the case of Cu_3Au, the Au atoms occupy the corner sites, while Cu atoms occupy the face centres of the basic cube; the opposite occurs for Au_3Cu. The simulation box contained 20 layers with 200 atoms each and periodic boundary conditions were applied in space. For the integration of the equations of motion we used a time step of 5 fs and the Verlet algorithm. Thermodynamical averages were computed over 50 ps trajectories after preliminary thermal equilibrium runs of 10 ps. At each temperature the lattice constant of the alloy was adjusted to a value resulting in zero pressure in the system. The atomic mean square displacements were deduced from the local-density profiles along a direction perpendicular to the atomic layers, while the phonon DOS was calculated by Fourier transforming the velocity auto-correlation function. Similar transformations were done in order to obtain the phonon spectral densities for a given polarization at a specific $\boldsymbol{k}$ vector in the first Brillouin zone and to also derive the phonon dispersion curves. Details of these calculational procedures are reported elsewhere [20, 27].

3. Results and discussion

In table 1 we give the calculated equilibrium lattice parameters and cohesive energies of the pure metals Cu, Au and their ordered alloys in the $L1_2$ structure, as well as the corresponding measured values [38–41]. The differences between predictions of lattice constants from the APW method and experimental values [38, 39] are very small, with the error ranging from 0.3% in Cu_3Au to 1.9% in Cu. Concerning the cohesive energies, we note a remarkable agreement with experiment for Au [40], while for Cu the error compared to experiment [40] is 31% due to the well known inaccuracy of the LDA approach for atoms. On the other hand, the computed cohesive energies of the alloys agree within 10% with the experimental data of [41].

Table 1. Calculated (Calc.) and experimental (Expt.) lattice parameters [38, 39], a, along with the cohesive energies E_c, for Cu, Au [40] and their $L1_2$ ordered alloys [41]. Note that the experimental lattice parameter of Au_3Cu refers to room temperature.

	a (Å)		E_c (eV)	
Compound	Calc.	Expt.	Calc.	Expt.
Cu	3.53	3.60	4.65	3.54
Cu_3Au	3.75	3.74	4.06	3.64
Au_3Cu	4.00	3.98	3.45	3.79
Au	4.06	4.07	3.77	3.78

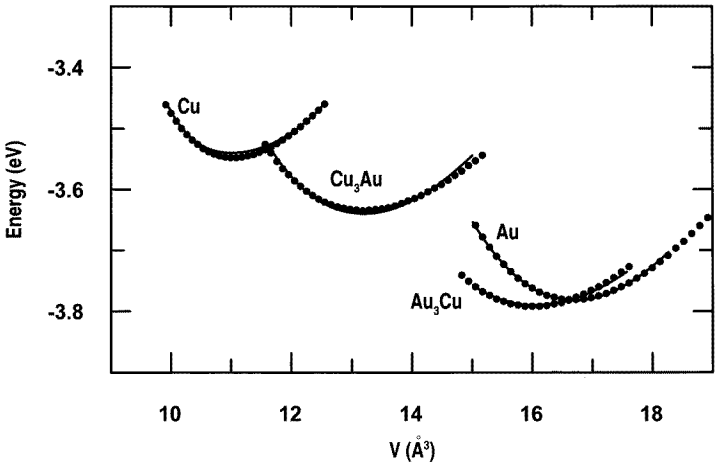

Figure 1. Volume dependence of the opposite of calculated cohesive energies per atom of Cu, Au, Cu_3Au and Au_3Cu. Solid lines refer to the APW results; filled symbols correspond to the results of the fit (equation (1)).

In figure 1 we plot the calculated cohesive energies per atom (with opposite sign) of the metals Cu, Au and their stoichiometric alloys Cu_3Au and Au_3Cu as a function of the volume (solid lines) after the energy shifts, so that at the minimum they give the experimental value of the corresponding cohesive energy. In the same graph we also show (with filled symbols) the results of the fit using the expression (1). We observe that this simultaneous fitting to the first-principles energy curves is almost perfect for all the systems under study. From

this adjustment we have obtained the 15 potential parameters of the expression (1) listed in table 2.

Table 2. Potential parameters of equation (1) obtained by fitting to the APW calculated volume dependence of the cohesive energies of Cu, Au, Cu_3Au and Au_3Cu.

$\alpha\beta$	$\xi_{\alpha\beta}$ (eV)	$A_{\alpha\beta}$ (eV)	$q_{\alpha\beta}$	$p_{\alpha\beta}$	$r_0^{\alpha\beta}$ (Å)
Au–Au	1.8241	0.2145	4.3769	10.8842	2.8652
Cu–Cu	1.2355	0.0862	2.3820	12.5785	2.4729
Cu–Au	1.7981	0.2356	2.6433	8.6961	2.6222

Table 3. Comparison between calculated and experimental values of bulk modulus B and elastic constants (in GPa) for Cu, Au and their $L1_2$ ordered alloys. The computations were performed within the SMA method and the experimental elastic constants were taken from [38].

	Calculated (GPa)				Experimental (GPa)			
Compound	B	C_{11}	C_{12}	C_{44}	B	C_{11}	C_{12}	C_{44}
Cu	142	180	122	86.8	137	168	121	75
Cu_3Au	137	166	122	69.3	151	189	132	73.6
Au_3Cu	169	197	155	58.9	166	189	155	47
Au	204	226	193	47.5	169	189	159	42

The above parameters have been used to calculate the bulk moduli and elastic constants of the pure metals and ordered $L1_2$ alloys. In table 3 we report these computed results, along with available experimental values [38]. The accuracy of these quantities is fairly good, since they differ from the experimental results by less than 20%. This is the same level of accuracy found in the first-principles linearized APW (LAPW) calculations and in the elaborate TB method results of [42]. In the case of the $L1_2$ alloys our computed bulk moduli for Cu_3Au and Au_3Cu are consistent with LAPW results [41] (140 and 194 GPa) and with augmented-spherical-wave calculations [43] (188 and 186 GPa) respectively.

We have also made a prediction of the cohesive energy of the CuAu (I) ordered alloy that crystallizes in $L1_0$ tetragonal structure with $c/a = 0.926$ [44]. By employing our parameters at the experimental ratio c/a, we deduced a cohesive energy, 3.72 eV, which agrees well with the value of 3.74 eV reported in [41].

A very good validation of the interatomic potential can be realized by performing MD simulations at various temperatures. In the case of pure metals, the present parameters give results similar to those we obtained in [27]. In figures 2(a) and 2(b) we present the computed temperature dependence of lattice constants of $L1_2$ ordered alloys, as well as available measurements [39, 45]. We see that the maximum lattice constant deviation between calculation and experiment in the case of Cu_3Au is only 0.25% at room temperature, while the differences are smaller as the temperature increases (figure 2(a)). Concerning Au_3Cu (figure 2(b)), we observe a disagreement of 1.04% in the lattice constant at room temperature. It should be noted here that our MD simulations do not show the order–disorder transition due to time limitations and the absence of defects [23].

In figures 3(a) and 3(b) we plot the atomic mean square displacements as a function of temperature (dashed lines) for Cu and Au atoms in the ordered alloys Cu_3Au and Au_3Cu, respectively, as obtained from our MD simulations, along with some low- and room-temperature experimental values [46]. Our results for Cu_3Au are in very good agreement

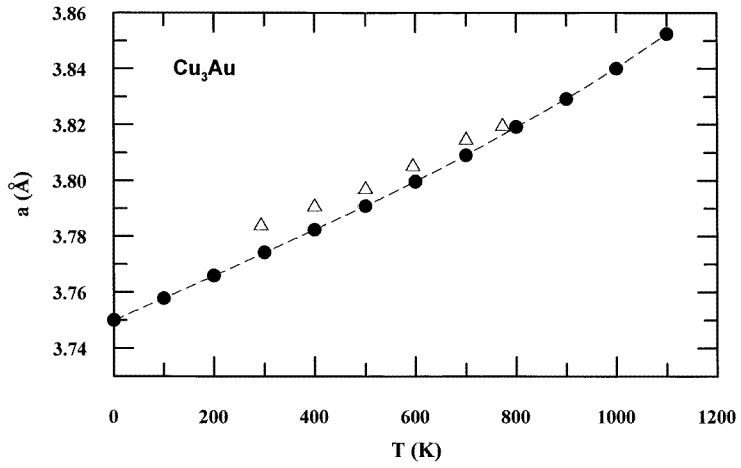

(a)

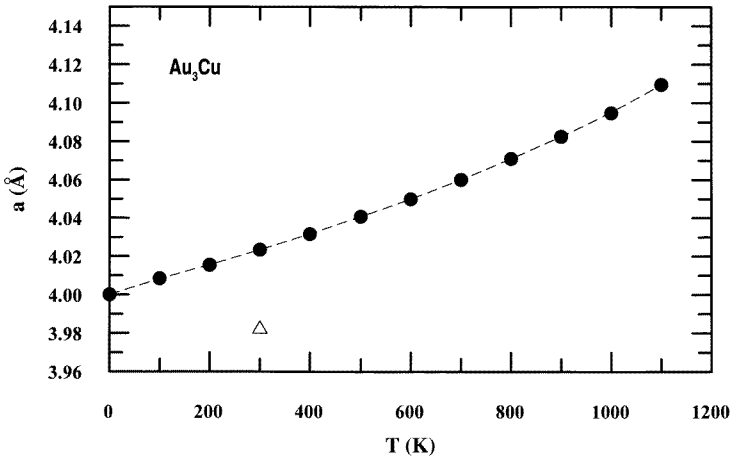

(b)

Figure 2. Lattice parameters of (a) Cu_3Au and (b) Au_3Cu as a function of temperature. The filled circles correspond to the results of the simulation, while the triangles to the experimental data from [45] and [39] for Cu_3Au and Au_3Cu respectively. The dashed lines are to guide the eye.

with the measured values (figure 3(a)), as well as with a previous MD simulation based on the same potential form, but resulting from fitting to experimental quantities [23]. In addition, our computed MSDs for Cu_3Au (figure 3(a)) are in satisfactory agreement with available averaged experimental data [47], 0.023 $Å^2$, just below the critical temperature of the order–disorder transition. From figures 3(a) and 3(b) it can be observed that the MSDs of Cu are larger than those of Au atoms in both ordered alloys. These results are in accordance with the low- and room-temperature measurements [46] as can be seen in figure 3(a). Furthermore, this finding is compatible with the experimental evidence using inelastic neutron scattering techniques that in ordered Cu_3Au the atomic Cu–Au force constants are five times stronger than the Cu–Cu force constants [48]. This difference between Cu–Au and Cu–Cu force constants can be attributed to the difference in the atomic

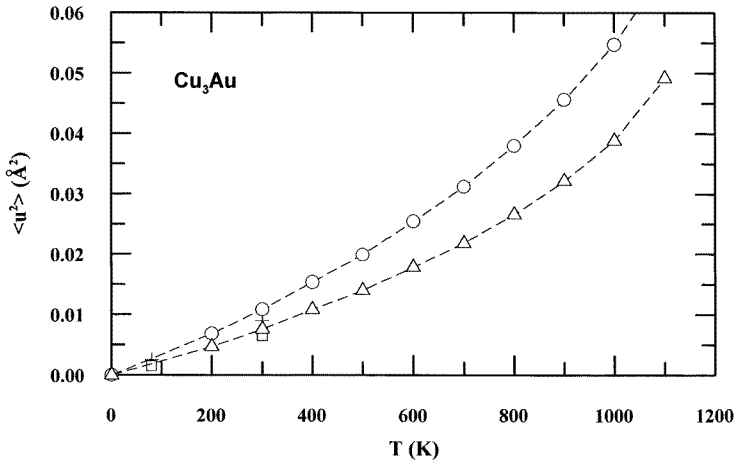

(a)

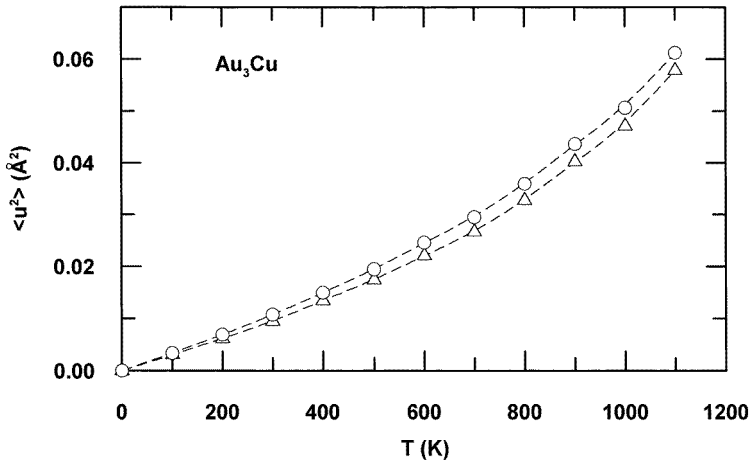

(b)

Figure 3. Temperature dependence of mean square displacements of (a) Cu_3Au and (b) Au_3Cu. The open circles and triangles correspond to the simulation results for Cu and Au atoms respectively. Experiment: crosses (Cu) and open squares (Au) from [46]. The dashed lines are to guide the eye.

radii of these ions—the radius of the Au ion is larger than that of the Cu ion—and to the internal energy of the system [48]. The difference between the vibrational amplitudes of each metal becomes more important in Cu_3Au as the temperature increases, while in Au_3Cu the two curves remain almost parallel, and close to each other. This also can be explained by the difference in force constants, in masses and in the geometry of the two alloys. To our knowledge the results for Au_3Cu are new in the literature.

The phonon densities of states for the two $L1_2$ alloys are shown in figures 4(a) and 4(b) at room temperature. In these plots we present our phonon frequency spectra for comparison using the parameters of table 2 (solid lines), along with the corresponding spectra using the parameters of [24] (filled circles), which have been deduced from fitting to

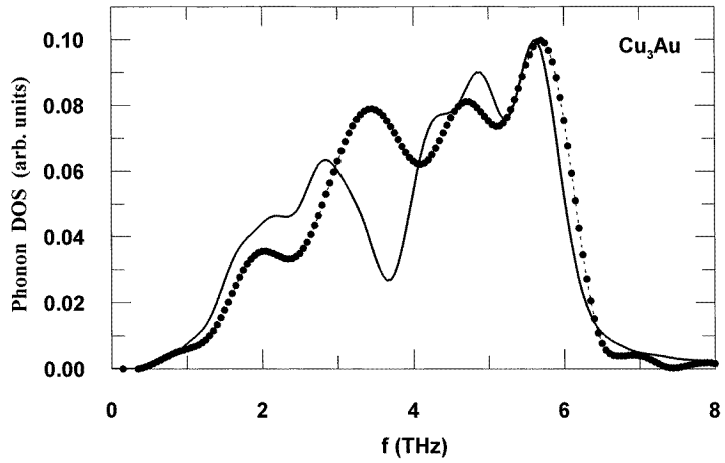

(a)

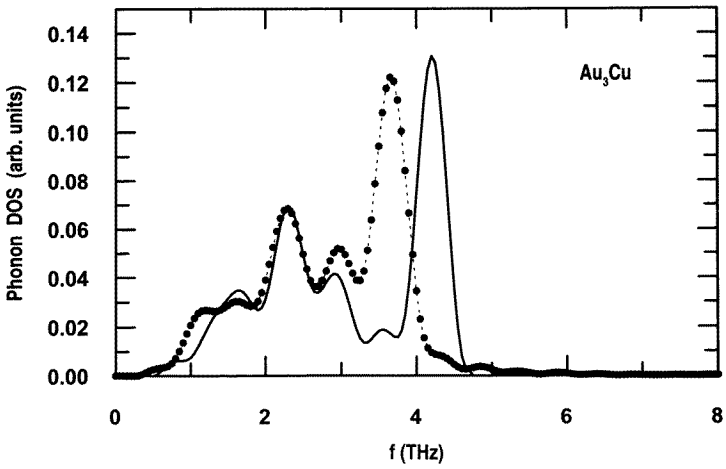

(b)

Figure 4. Phonon DOS of (a) Cu_3Au and (b) Au_3Cu at 300 K. Solid lines refer to our MD results using the parameters of table 2; filled circles correspond to MD results using those of [24].

experimental quantities. It should be noted here that the DOS shapes are smooth and without sharp discontinuities, because they were computated by a Fourier transform of the velocity autocorrelation function. The phonon spectra of both ordered alloys contain several modes denoting the strong interactions between Cu and Au and they are very different compared with those of pure metals [27]. Comparing our phonon spectra with those calculated from the data of [24], we observe a reasonable agreement for the cutoff frequency and most modes, except for a shift of 0.5 THz toward lower frequencies in the centre of the spectrum for Cu_3Au and higher frequencies in the right part of spectrum for Au_3Cu. These differences could be resolved by direct comparison with the measured phonon DOS which are not available. Our phonon DOS for Cu_3Au is also in satisfactory agreement with that of [22], in which a fitting of SMA parameters to experimental data has also been done.

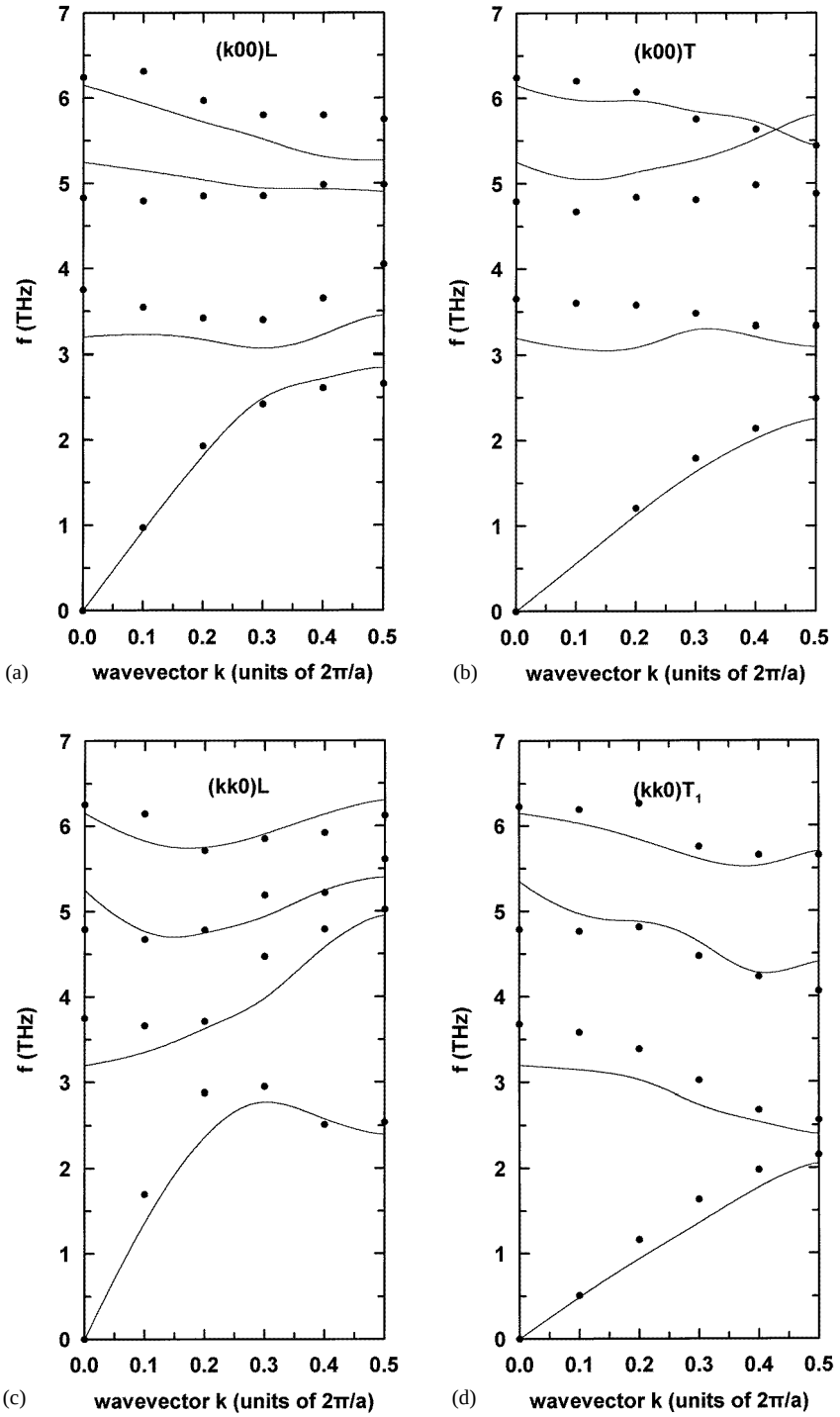

Figure 5. Phonon-dispersion curves of ordered Cu_3Au at 300 K for (a), (b) the [100], (c), (d), (e) the [110], and (f), (g) the [111] directions. Solid lines correspond to MD simulations after a cubic spline interpolation; filled circles refer to the experimental results from [48].

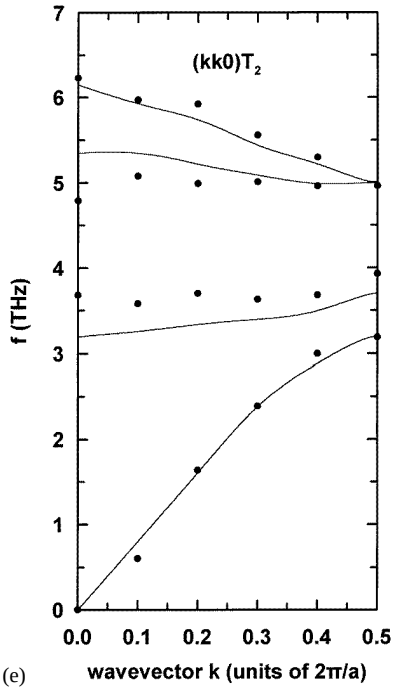

(e)

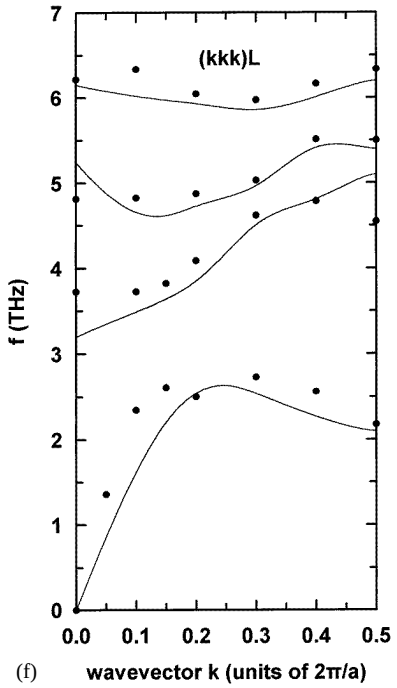

(f)

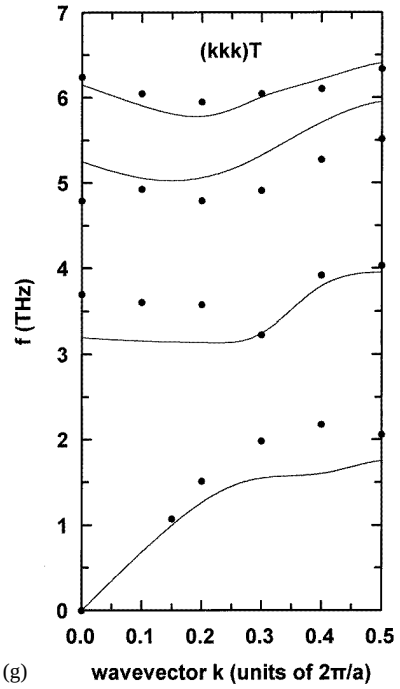

(g)

Figure 5. (Continued)

The phonon-dispersion curves of ordered Cu_3Au along the high-symmetry [100], [110] and [111] directions at room temperature are presented in figures 5(a)–5(g), together with

the experimental data using inelastic neutron scattering techniques [48]. The agreement between simulation and measurements is fairly satisfactory, except for the crossing of modes along the [100] direction in the high-frequency region, figure 5(b) (transverse phonons T). This feature also has been found in [22], where the SMA approach has been applied by fitting to experimental quantities. We note that there is a remarkable agreement with the experiment [48] in the value of the splitting between the transverse acoustic and optical modes in the [111] direction (figure 5(g)): this gap was found to be 8.9 meV, compared to the experimental value of 8 meV. However, there is a discrepancy with [22] where a gap of only 3.5 meV is reported. This result supports the procedure of obtaining the SMA parameters from first-principles total-energy data rather than experimental quantities.

4. Conclusions

We presented an alternate approach of determining the parameters of interatomic potentials of Cu, Au and Cu–Au $L1_2$ ordered alloys within the second-moment approximation of the tight-binding theory by adjusting to the total-energy APW calculations as a function of volume. This scheme provided fairly accurate results for the bulk modulus, elastic constants of pure metals and ordered alloys, and predicted a correct cohesive energy for the tetragonal $L1_0$ CuAu alloy. Furthermore, we used this interatomic potential to perform finite-temperature molecular-dynamics simulations and found that the lattice constants and the atomic mean square displacements of stoichiometric alloys determined as a function of temperature are in good agreement with measurements. Finally, we obtained the phonon spectra and phonon dispersion curves with accuracy comparable to that found by the standard SMA, in which the parameters are fitted to several experimental data. An extension of the above described procedure to disordered alloys should be very useful in investigating changes of the vibrational properties upon disorder.

Acknowledgments

This work was supported by a NATO grant No CRG-940118 and a grant N00014-98-1-4024 from the Department of the Navy issued by the Office of Naval Research International Field Office—Europe. The United States has a royalty-free license throughout the world in all copyrightable materials contained herein.

References

[1] Meyer M and Pontikis V (eds) 1991 *Computer Simulation in Materials Science* (Dordrecht: Kluwer)
[2] Allen M P and Tildesley D J (eds) 1993 *Computer Simulation in Chemical Physics* (Dordrecht: Kluwer)
[3] Kirchner H O, Kubin L P and Pontikis V (eds) 1996 *Computer Simulation in Materials Science* (Dordrecht: Kluwer)
[4] Mark J E, Glicksman M E and Marsh S P (eds) 1992 *Mater. Res. Soc. Symp. Proc.* vol 278 (Pittsburgh, PA: Materials Research Society)
[5] Bronghton J, Bristowe P and Newsam J 1993 *Mater. Res. Soc. Symp. Proc.* vol 291 (Pittsburgh, PA: Materials Research Society)
[6] Car R and Parrinello M 1985 *Phys. Rev. Lett.* **55** 2471
[7] Sutton A P and Balluffi R W 1995 *Interfaces in Crystalline Materials* (Oxford: Oxford University Press) ch 3
[8] Raeker T J and DePristo A E 1991 *Int. Rev. Phys. Chem.* **93** 1
[9] Daw M S and Baskes M I 1984 *Phys. Rev.* B **29** 6443
Foiles S M, Baskes M I and Daw M S 1986 *Phys. Rev.* B **33** 7983
[10] Nørskov J K 1990 *Rep. Prog. Phys.* **53** 1253

[11] Finnis M W and Sinclair J E 1984 *Phil. Mag.* A **50** 45
[12] Ercolessi F, Tosatti E and Parinello M 1986 *Surf. Sci.* **177** 314
Ercolessi F, Tosatti E and Parinello M 1986 *Phys. Rev. Lett.* **57** 719
[13] Ducastelle F 1970 *J. Physique* **31** 1055
Ducastelle F and Cyrot-Lackmann F 1971 *J. Phys. Chem. Solids* **32** 285
[14] Tomanek D, Aligia A A and Balseiro C A 1985 *Phys. Rev.* B **32** 5051
Zhong W, Li Y S and Tomanek D 1991 *Phys. Rev.* B **44** 13 053
[15] Rosato V, Guillope M and Legrand B 1989 *Phil. Mag.* A **59** 321
[16] Sutton A P 1994 *Electronic Structure of Materials* (Oxford: Oxford University Press) ch 9
[17] Cleri F and Rosato V 1993 *Phys. Rev.* B **48** 22
[18] Loisel B, Gorse D, Pontikis V and Lapujoulade J 1989 *Surf. Sci.* **221** 365
[19] Loisel B, Lapujoulade J and Pontikis V 1991 *Surf. Sci.* **256** 242
[20] Papanicolaou N I, Lagaris I E and Evangelakis G A 1995 *Surf. Sci.* **337** L819
[21] Evangelakis G A and Papanicolaou N I 1996 *Surf. Sci.* **347** 376
[22] Cleri F and Rosato V 1993 *Phil. Mag. Lett.* **67** 369
[23] Rey-Losada C, Hayoun M and Pontikis V 1993 *Mater. Res. Soc. Symp. Proc.* vol 291 (Pittsburgh, PA: Materials Research Society) p 549
[24] Dumez C, Hayoun M, Rey-Losada C and Pontikis V 1994 *Interface Sci.* **2** 45
[25] Polatoglou H M and Bleris G L 1994 *Interface Sci.* **2** 31
[26] Polatoglou H M and Bleris G L 1994 *Solid State Commun.* **90** 425
[27] Kallinteris G C, Papanicolaou N I, Evangelakis G A and Papaconstantopoulos D A 1997 *Phys. Rev.* B **55** 2150
Sigalas M M and Papaconstantopoulos D A 1994 *Phys. Rev.* B **49** 1574
[28] Sham T K, Hiraya A and Watanabe M 1997 *Phys. Rev.* B **55** 7585 and references therein
[29] Mattheiss L F, Wood J H and Switendick A C 1968 *Methods Comput. Phys.* **8** 63
Sigalas M, Papaconstantopoulos D A and Bacalis N C 1992 *Phys. Rev.* B **45** 5777
Sigalas M M and Papaconstantopoulos D A 1994 *Phys. Rev.* B **50** 7255
[30] Hedin L and Lundqvist B I 1971 *J. Phys. C: Solid State Phys.* **4** 2064
[31] Kohn W and Sham L J 1965 *Phys. Rev.* A **140** 1133
[32] Hohenberg P and Kohn W 1964 *Phys. Rev.* B **136** 864
[33] Koelling D D and Harmon B N 1977 *J. Phys. C: Solid State Phys.* **10** 3107
[34] Janak J F 1974 *Phys. Rev.* B **9** 3985
[35] Birch F 1978 *J. Geophys. Res.* **83** 1257
[36] Evangelakis G A, Rizos J P, Lagaris I E and Demetropoulos I N 1987 *Comput. Phys. Commun.* **46** 401
[37] Mehl M J, Osburn J E, Papaconstantopoulos D A and Klein B M 1990 *Phys. Rev.* B **41** 10 311
Mehl M J, Klein B M and Papaconstantopoulos D A 1994 *Intermetallic Compounds: vol 1, Principles* ed J H Westbrook and R L Fleischer (New York: Wiley) p 195
[38] Simmons G and Wang H 1971 *Single Crystal Elastic Constants and Calculated Aggregate Properties: a Handbook* 2nd edn (Cambridge, MA: MIT Press)
[39] Wright P and Goddard K F 1959 *Acta Metall.* **7** 757
[40] Kittel C 1966 *Introduction to Solid State Physics* 3rd edn (New York: Wiley)
[41] Wei S-H, Mbaye A A, Ferreira L G and Zunger A 1987 *Phys. Rev.* B **36** 4163
[42] Mehl M J and Papaconstantopoulos D A 1996 *Phys. Rev.* B **54** 4519
[43] Terakura K, Oguchi T, Mohri T and Watanabe W 1987 *Phys. Rev.* B **35** 2169
[44] Taylor A and Kagle B J 1963 *Crystallographic Data on Metal and Alloy Structures* (New York: Dover)
[45] Pearson W B 1967 *A Handbook of Lattice Spacings and Structures of Metals and Alloys* (Oxford: Pergamon)
[46] Schwartz L H and Cohen J B 1965 *J. Appl. Phys.* **36** 598
[47] Lander G H and Brown P J 1985 *J. Phys. C: Solid State Phys.* **18** 2017
[48] Katano S, Iizumi M and Noda Y 1988 *J. Phys. F: Met. Phys.* **18** 2195